Catalysis Letters
https://doi.org/10.1007/s10562-022-04107-y

Methanol Oxidation Catalytic Performance Enhancement via Constructing Pd-$MgAl_2O_4$ Interface and its Reaction Mechanism Investigation

Wei Zhao[1] · Hongyi Zhang[2] · Lei Zhang[3] · Jianchao Gong[1] · Tianen Chen[1] · Liming Ren[4] · Yaxiong Ji[1,5] · Fanbin Meng[4]

Received: 29 March 2022 / Accepted: 6 July 2022

Abstract

The methanol oxidation reaction is a promising route to eliminating trace amount of methanol in exhaust gases which aroused serious environmental concern. In this work, a novel Pd/$MgAl_2O_4$ catalyst was prepared to construct the metal-support interface and employed in the methanol oxidation reaction. The reaction results show that the Pd/$MgAl_2O_4$ catalyst could achieve 100% methanol oxidation at 198 ℃ over the Pd/MgO and Pd/Al_2O_3 catalysts. The high-resolution transmission electron microscopy (HRTEM), X-ray diffraction (XRD), CO-chemisorption, H_2 temperature programmed reduction (H_2-TPR), and CO diffuse reflectance infrared Fourier transformed spectroscopy (CO-DRIFTS) show that the Pd was uniformly distributed over the $MgAl_2O_4$ support due to strong interaction between Pd and $MgAl_2O_4$. The mechanism studies show that the abundant Pd-$MgAl_2O_4$ interfaces significantly contributed to the reaction enhancement. The Pd-$MgAl_2O_4$ interfaces could greatly enhance the oxidation reaction at a lower temperature with the assistance of oxygen vacancies compared with traditional oxide catalysts, which was confirmed by methanol temperature program surface reaction (MeOH-TPSR) experiments. *In-situ* DRIFTS is carried out to elucidate the reaction mechanism and establish the structure – activity relationship: the methanol could be effectively absorbed on the $MgAl_2O_4$ support with oxygen vacancies to form bidentate formate, then the Pd species assisted the intermediates converting to CO_2 product. The Pd/$MgAl_2O_4$ catalyst and its enhancement mechanism investigation provided a potential strategy in the VOCs removal catalysis development.

Graphical Abstract

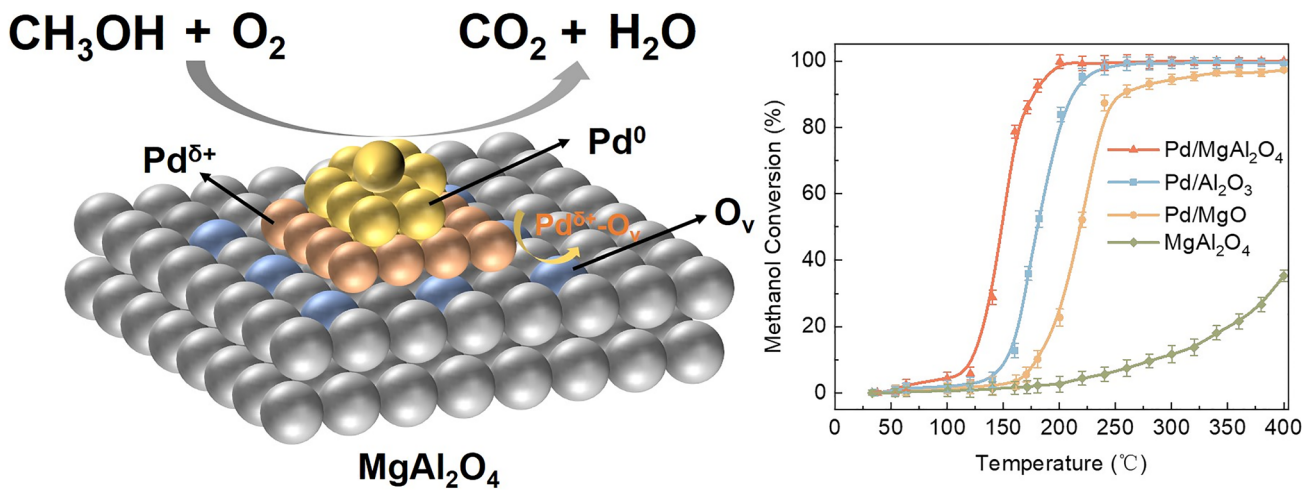

Wei Zhao and Hongyi Zhang have contributed equally to this work.

Extended author information available on the last page of the article

Published online: 25 July 2022

Keywords Methanol oxidation · Pd · $MgAl_2O_4$ · Metal-support interface

1 Introduction

Volatile organic compounds (VOCs) have been regarded as serious air pollution and cause breathing discomfort, triggering allergies and asthma diseases [1, 2]. Methanol, which is characterized by high vapor pressure and lower water solubility, is one of the representative VOCs species [3, 4]. Furthermore, complete oxidation methanol reaction could provide a strategy for VOCs removal catalysts development because methanol molecule (CH_3OH) is with different chemical bonds, such as C = O, C-H, and O–H. Thus, the methanol oxidation reaction and its mechanism studies could effectively contribute to the VOCs removal application and its academic understanding.

Novel metal is usually employed to construct the high-performance catalyst for the complete oxidation reaction [2, 3, 5, 6]. Generally, the metal-support interface would significantly contribute to the catalytic performance in different reactions [7]. For the oxidation reactions, the oxygen vacancy defect would assist the VOCs to absorb on the support, forming intermediates, and the novel metal species accelerates the intermediates converting to CO_2 product in the oxygen atmosphere [8–10]. Different oxides have been widely employed as supports to tune the structural and electronic properties of metal-oxide interface to enhance the catalytic performance. Besides traditional oxide, the metal organic frameworks (MOFs) [11, 12], molecular sieve [13–15], and carbon nano-tube (CNT) [16] are also used for the complete oxidation reaction catalysts preparation. Even though a series of outstanding catalytic performances have been achieved, a more efficient catalyst with lower reaction temperature was desired to be developed under a stricter environmental protection requirement.

The spinel oxide, which is a class of minerals with general formulation AB_2X_4, has been applied to different reactions due to its unique properties [17, 18]. The benefits of spinel oxides, such as their controllable composition, structure, valence, and morphology, would increase their catalytic performance in various reactions. For example, $ZnFe_2O_4$ could regulate copper sites for CO_2 hydrogenation to methanol [18]. And the formation of spinel $CuAl_2O_4$ and $MgAl_2O_4$ was reported that it could increase the methanol selectivity via increasing the amount of active basic sites [19]. A novel Cu-Mn-O nano-particle/nano-sheet spinel-type catalyst was used in the methanol steam reforming (MSR) and preferential oxidation (PROX) reaction for purified hydrogen production. The spinel-type catalyst presented a superior catalytic activity due to its higher O_2 adsorption/storage capacity from the abundant surface defects [20]. Furthermore, spinel catalysts have also been used to facilitate NO_x reduction [21], CO oxidation [22], chemical looping combustion (CLC) [23], and NH_3 oxidation reactions [24], et al. Given the above researches, enhancing methanol oxidation performance by preparing catalysts used spinel oxide as support to construct metal-support interface is a strategy. And a series of mechanism characterizations (MeOH-TPSR, *in-situ* DRFITS studies, et al.) would establish the structure – activity relationship, providing more information for further catalysis development [25–28].

In this work, the spinel oxide ($MgAl_2O_4$) was used as the support for Pd species in methanol oxidation, forming abundant Pd-$MgAl_2O_4$ interfaces due to a strong metal-support interaction. The HRTEM, XRD, BET, H_2-TPR, CO-DRIFTS were carried out to characterize its textural properties. The MeOH-TPSR was used to investigate the oxidation ability without oxygen and *in-situ* DRIFTS were employed to investigate methanol oxidation reaction mechanism under real reaction conditions. This work provides new insight into the effect of novel metal and spinel oxide interface on methanol oxidation and offers a strategy to design a more active catalyst for industrial application.

2 Experimental Section

2.1 Catalyst Preparation

2.1.1 Materials

Aluminium nitrate nonahydrate, magnesium nitrate hexahydrate, γ-aluminum oxide, magnesium oxide, palladium chloride, ammonium chloride, citric acid monohydrate, and ethanol were supplied by Shanghai aladdin Biochemical Technology Co.,Ltd. All of the above chemicals were used without further purification.

2.1.2 Catalyst Preparation

The $MgAl_2O_4$ was prepared by sol–gel method as catalyst support. $Mg(NO_3)_2{\cdot}6H_2O$ (2.5640 g, 10 mmol), $Al(NO_3)_3{\cdot}9H_2O$ (7.5026 g, 20 mmol), and $C_6H_{10}O_8$ (9.4563 g, 60 mmol) were dissolved in 100 mL water with 90 ℃ and vigorous stirring. The formed gel was dried in an oven at 100 ℃ overnight, and the dried sample was calcined at 800 ℃ for 7 h under air.

The Pd/$MgAl_2O_4$, Pd/MgO, and Pd/Al_2O_3 catalysts with Pd loading of 1 wt% were prepared by the impregnation method. Stoichiometric palladium chloride and ammonium chloride citric (the molar ratio of NH_4Cl: $PdCl_2$ = 10:1) were added to ethanol with 80 ℃ and vigorous stirring until the

water has evaporated completely. The impregnated samples were dried at 100 ℃ overnight. After calcinating at 400 ℃ for 5 h under air, the preparation of the catalyst was finished.

2.2 Catalyst Characterization

2.2.1 Structural Characterizations

The catalyst crystal structures were confirmed by an X ray diffractometer (XRD) equipment with a Cu Kα X-ray source at a step size of 0.01° (MiniFlex 600, Rigaku, Japan). The surface area measurements were analyzed by nitrogen adsorption instrument (ASAP 3020, Micromeritics, USA) with BET analysis method. The sample was degassed under vacuum at 200 ℃ for 2 h. The size and the morphology of the Pd particles were studied and analyzed on the electron microscope (FEI Tecnai 30, FEI, USA), which was equipped with a high-angle annular dark field scanning transmission electron microscopy (HAADF-STEM) detector. H_2 temperature-programmed reduction (H_2-TPR) was conducted at a chemisorption analyze (AutoChem II 2920, Micromeritics, USA) with thermal conductivity detector (TCD). 100 mg of samples was reduced in 10% H_2 mixture with He at 50 ml/min flowrate. The temperature was controlled from 20 to 800 °C at a heating rate of 10 °C min^{-1}. The actual Pd weight percentage was determined by an inductively coupled plasma – optical emission spectroscopy (ICP-OES) (Spectro Arcos, SPECTRO, German). CO chemisorption was carried out at a chemisorption analysis (AutoChem II 2920, Micromeritics, USA). 100 mg of samples were reduced in 10% H_2 mixture with He at 50 ml/min flowrate for 120 min at 300 °C. After purged with Ar flow for 10 min, 200 pulses of CO via a gas loop of 50 μL were used to determine the metal dispersion. The metallic Pd area was calculated as follows:

$$S_{\mathrm{Pd}}\left(m^2/g\right) = \frac{D_{\mathrm{Pd}} \times N_a}{M_{\mathrm{Pd}} \times S_a} \tag{1}$$

where D_{Pd} is the Pd dispersion; N_a is the Avogadro constant, 6.02×10^{23}; M_{Pd} is the atomic weight of Pd, 106.42 g/mol; S_a is the amount of Pd atom per square meter, 1.27×10^{19} atom/m^2.

2.2.2 Mechanism Studies

The methanol temperature-programmed surface reaction (MeOH-TPSR) was conducted in a fixed bed with 30 mg catalysts, which was equipped with a Fourier Transform infrared spectroscopy (FTIR) (iS20, Nicolet, USA) to detect the product. The methanol vapor was fed into the reactor with 100 ml/min of N_2. The temperature was controlled from 50 to 400 °C at a heating rate of 10 °C min^{-1}. The CO-DRIFTS experiments were carried out via a FTIR (iS50, Nicolet, USA) equipped with a Mercury-Cadmium-Telluride (MCT) detector. The catalysts diluted by quartz sand were pressed into thin wafers and placed in a reaction chamber with a ZnSe window. Prior to CO adsorption, the catalysts were reduced with 20 ml/min of H_2 at 200 °C for 1 h. Then the gas was switched as follows: (i) a continuous CO flow of 20 ml/min was entered into the cell, and (ii) N_2 was used to purge after saturation coverage was reached. The IR spectra was recorded via recording 64 scans with a resolution of 4 cm^{-1}.

2.3 Reaction Performance Evalution and *In-Situ* Studies

The methanol oxidation catalytic performance were carried out in a fixed bed reactor. The catalysts (60–80 mesh) of 30 mg was packed into the reactor. The reaction temperature was controlled by a pair of thermocouples placed near the catalyst bed connected to the temperature controller. The methanol vapor was generated by a set of bubbling columns at a constant temperature (0 ℃), and fed to the reactor with 100 ml/min Ar and 20 ml/min synthetic air (20 vol.% O_2 in N_2, Air Products). The reaction temperature was carried out from 30 to 400 °C. The methanol conversion was measured by an online gas chromatograph (Agilent 6890) with a pair of thermal conductivity and flame ionization detectors (TCD and FID). The methanol conversion was calculated as follows:

$$\text{MeOH Conversion } (\%) = \frac{[\mathrm{MeOH}]_{\mathrm{in}} - [\mathrm{MeOH}]_{\mathrm{out}}}{[\mathrm{MeOH}]_{\mathrm{in}}} \tag{2}$$

where $[\mathrm{MeOH}]_{\mathrm{in}}$ and $[\mathrm{MeOH}]_{\mathrm{out}}$ are the steady-state concentrations of methanol at the reactor inlet and outlet for a given reaction temperature. Before the catalytic performance evaluation, the tightness of the pipe was tested via building the pressure. The measurement point at the same temperatures was introduced to the gas chromatograph three times for the average calculation with a carbon mass balance of above 98%.

In-situ DRIFTS experiments were carried out via a FTIR (iS50, Nicolet, USA) equipped with MCT detector. The catalysts diluted by quartz sand were pressed into thin wafers and placed in a reaction chamber with a ZnSe window. Different gas (methanol vapor or air) was fed into the reactor at 200 ℃ to detect the intermediates species and its reaction behaviors. First, the methanol vapor was entered into the reactor for 30 min, then the oxygen gas was switched, which was maintained 30 min. The IR was accumulated by recording 64 scans with a resolution of 4 cm^{-1}.

3 Results and Discussion

3.1 Structural Properties

To investigate the crystalline phases of the prepared catalysts, the XRD patterns were depicted in Fig. 1a-c. In the XRD patterns, the main diffraction peaks of three catalysts were in good agreement with standard diffraction data, which suggested that the sol–gel with impregnation method could successfully prepare the $Pd/MgAl_2O_4$ catalyst. The average crystalline sizes were determined via Scherrer equation: $Pd/MgAl_2O_4$ catalyst (about 68 nm) and Pd/Al_2O_3 catalyst (about 63 nm) was significantly smaller than that of Pd/MgO catalyst (about 200 nm). A smaller particle size of the $Pd/MgAl_2O_4$ catalyst would contribute to the metal dispersion, thus affecting the oxidation activities. It is noteworthy that the diffraction peaks of three catalysts after reaction kept the same intensity with the fresh catalysts, which showed good thermal stability of all catalysts. For all of catalysts ($Pd/MgAl_2O_4$, Pd/MgO and Pd/Al_2O_3 catalyst), no PdO diffraction peaks were observed in the XRD patterns due to their small particle size, which suggests the metal-support interfaces were generated over the catalysts.

The pore structure of catalysts was detected by N_2 adsorption isotherms shown in Fig. 1d and listed in Table 1. All of catalysts demonstrated the characteristics of mesoporous structures. The specific surface area of $Pd/MgAl_2O_4$ (105.8 m^2/g) and Pd/Al_2O_3 (145.2 m^2/g) were higher than Pd/MgO (35.9 m^2/g), which indicates that the spinel oxide could be excellent catalytic support for the preparation of the catalyst. The BJH pore size distributions of sorbents are shown in Figure S1. From the BJH pore-size distribution curves

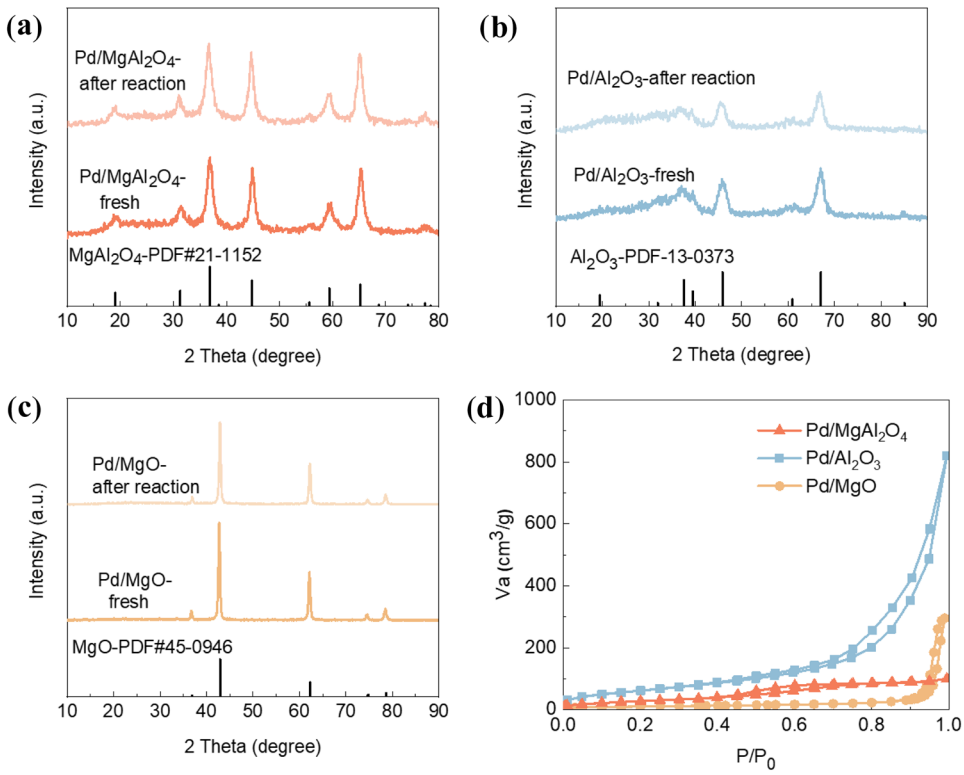

Fig. 1 XRD patterns of **a** $Pd/MgAl_2O_4$ catalyst; **b** Pd/Al_2O_3 catalyst; **c** Pd/MgO catalyst, and **d** N_2 adsorption–desorption isotherms of different catalysts

Table 1 Textural properties of different catalysts

Catalysts	S_{BET} (m^2/g) [a]	V_{pore} (cm^3/g) [a]	d_{pore} (nm) [a]	Pd dispersion (%) [b]	Pd metallic area (m^2/g) [b]
$Pd/MgAl_2O_4$	105.8	0.16	10.9	55.4	246.8
Pd/Al_2O_3	145.2	0.93	30.4	37.9	168.8
Pd/MgO	35.9	0.27	27.8	29.3	130.5

[a]Calculated from N_2 adsorption–desorption isotherms according to BET and BJH methods

[b]Determined by CO chemisorption

obtained from the desorption branch, the Pd/$MgAl_2O_4$ catalyst has a smaller pore size of 10.9 nm than that of the Pd/Al_2O_3 (30.4 nm) and Pd/MgO (27.8 nm) catalysts. The smaller pore size would increase the specific surface area, which benefits its metal dispersion for the catalytic performance improvement.

The distribution of Pd particles over the catalyst is studied by HAADF-STEM images. As shown in Fig. 2a, the Pd particles were randomly distributed over $MgAl_2O_4$ and the particle size distribution was mostly within 1–3 nm with a mean size of 2.0 nm. However, Pd particles on Al_2O_3 and MgO had a larger particle size and tended to agglomeration (Fig. 2b, c). The Pd particle sizes were 2.6 nm over MgO and 2.4 nm over Al_2O_3. The smaller Pd particle size of Pd/$MgAl_2O_4$ catalyst would benefit the generation of metal-support interfaces when compared with that of Pd/Al_2O_3 and Pd/MgO catalyst. The Pd dispersion behaviors were confirmed via CO-chemisorption characterization, agreeing with the HAADF-STEM results: the Pd/$MgAl_2O_4$ catalyst has a higher Pd dispersion of 55.4% than that of Pd/Al_2O_3 catalyst (37.9%) and Pd/MgO catalyst (29.3%). The metallic area of Pd was calculated via the Pd dispersion (Table 1): Pd/$MgAl_2O_4$ catalyst has a higher Pd metallic area of 246.76 m^2/g than that of Pd/Al_2O_3 catalyst (168.81 m^2/g) and Pd/MgO catalyst (130.51 m^2/g).

The highly uniform dispersion of Pd species over $MgAl_2O_4$ would significantly contribute to the catalytic performance due to its abundant active sites.

3.2 Catalytic Performance

The catalysts were tested for the methanol oxidation. During the reaction, no other products were detected except CO_2 and H_2O, which showed the reforming reactions could not happen with excess oxygen in the system. Figure 3a presents different methanol oxidation performances of Pd/$MgAl_2O_4$ catalyst, Pd/MgO catalyst, Pd/Al_2O_3 catalyst, and $MgAl_2O_4$ support. Besides complete conversion temperature, T50 (the temperature needed to reach 50% methanol conversion) and T90 (the temperature needed to obtain 90% methanol conversion) were parameters frequently used to characterize the activity of the methanol oxidation [13]. As shown in Fig. 3a, the methanol oxidation reaction could be occurred over pure $MgAl_2O_4$ support. It is suggested that the abundant oxygen vacancies in the spinel oxide could catalyze the reaction, which had been verified in previous references [29, 30]. However, its catalytic performance was at a lower level: 40% of methanol conversion was achieved at 400 ℃, which could not reach the environmental protection requirements. When Pd species was supported on $MgAl_2O_4$, the catalytic performance had a significant enhancement. The Pd/$MgAl_2O_4$ catalyst begins to be active to oxidize methanol at 75 ℃, reaching 50% conversion at 148 ℃ and 90% conversion at 175 ℃, and the Pd/$MgAl_2O_4$ catalyst could achieve 100% methanol oxidation at 198 ℃. Compared with pure $MgAl_2O_4$ support, the better catalytic performance of Pd/$MgAl_2O_4$ catalyst suggests that the abundant Pd-$MgAl_2O_4$ interfaces with highly distributed Pd species could greatly enhance the reaction performance. For Pd supported on traditional oxide supports, T50 and T90 were 180 ℃ and 215 ℃ for Pd/Al_2O_3 catalyst, and T50 and T90 were 220 ℃ and 256 ℃ for Pd/MgO catalyst. When compared with other reported catalysts in the references as shown in Table 2, the catalytic performance of Pd/$MgAl_2O_4$ catalyst exhibits a good activity over literature reported perovskite-type, zeolites-type, and traditional oxide-based catalysts in the methanol oxidtion reaction. The lower complete conversion temperature over Pd/$MgAl_2O_4$ catalyst shows a huge industrial application potential with a higher energy efficiency.

3.3 Mechanism Studies

3.3.1 H_2-TPR Characterization

The H_2-TPR characterization could be used to illustrate the interactions between metal and supports. Figure 4 shows the H_2-TPR profiles of Pd/$MgAl_2O_4$ catalyst, Pd/MgO catalyst, Pd/Al_2O_3 catalyst, and $MgAl_2O_4$ support. As shown in the TPR profiles, two hydrogen consumption peaks could be observed. The reduction peak that occurred at lower temperature was assigned to the highly dispersed PdO species. The other peak at higher temperature was regarded to the larger particles on the support [31]. The amount of H_2 consumed during H_2-TPR was calculated by employing the high purity of CuO as a standard sample. The consumption of H_2 over the three catalysts is almost the same, indicating that the content of Pd in the three catalysts are consistent. The deconvolution of peaks between 60 and 90 ℃ was calculated and the ratio of this peak area was also listed in Table S1. The Pd/$MgAl_2O_4$ catalyst has the lowest ratio of peak area between 60 and 90 ℃ over three catalysts (Pd/$MgAl_2O_4$: 52.8%; Pd/Al_2O_3: 61.4%; Pd/MgO: 83.9%), suggesting that Pd species on the $MgAl_2O_4$ support mainly exist in the form

Table 2 Catalytic performance over different catalysts

Catalysts	T50(°C)	T90(°C)	Ref
1%Pd/NaY	192	205	[12]
1%Pd/HY	170	192	[12]
1%Ag/$La_{0.6}Sr_{0.4}MnO_3$	155	172	[29]
6%Ag/γ-Al_2O_3	135	175	[29]
Cu/Li_2O/Al_2O_3	370	–	[30]
Pd/$MgAl_2O_4$	148	175	This work
Pd/Al_2O_3	180	215	This work
Pd/MgO	220	256	This work

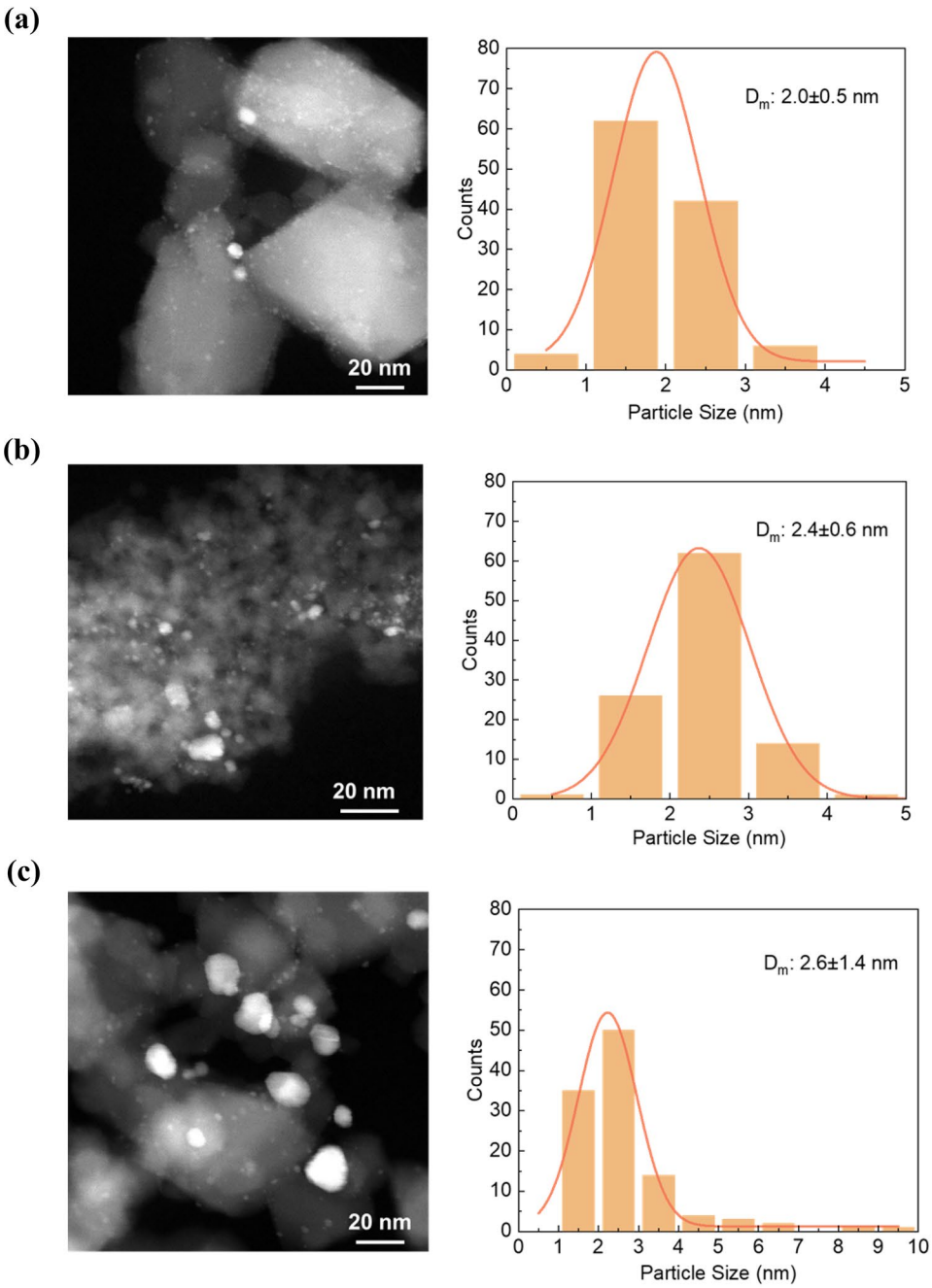

Fig. 2 HAADF-STEM images and corresponding Pd particle size distribution profiles of the reduced Pd catalysts: **a** Pd/$MgAl_2O_4$ catalyst; **b** Pd/Al_2O_3 catalyst; **c** Pd/MgO catalyst

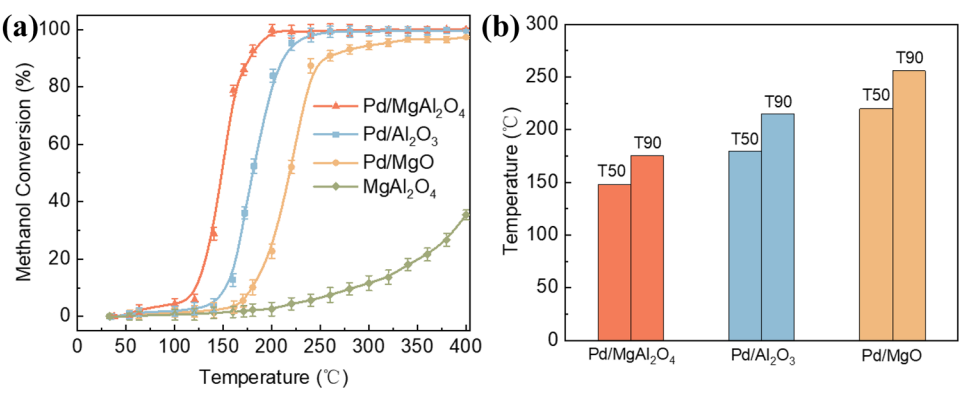

Fig. 3 **a** Catalytic performance and **b** T50 and T90 over Pd/$MgAl_2O_4$ catalyst, Pd/MgO catalyst, and Pd/Al_2O_3 catalyst

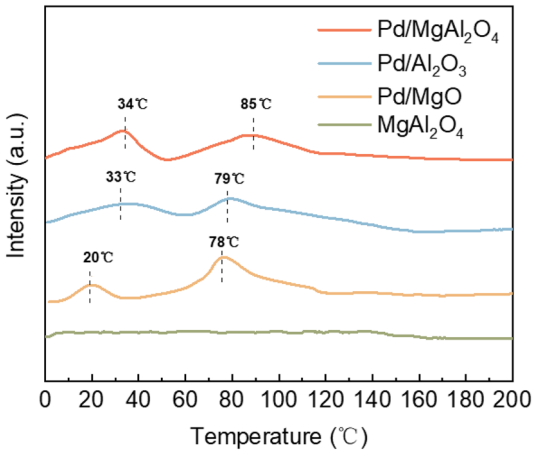

Figure. 4 H_2-TPR profiles of Pd/$MgAl_2O_4$ catalyst, Pd/Al_2O_3 catalyst, and Pd/MgO catalyst

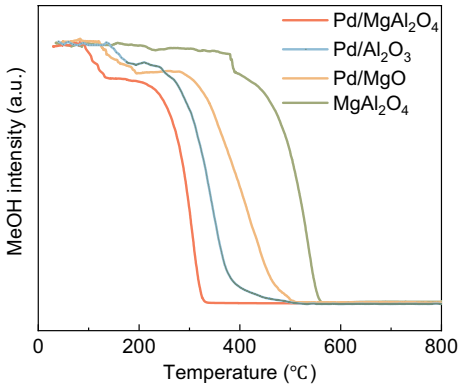

Fig. 5 MeOH-TPSR profiles of Pd/$MgAl_2O_4$ catalyst, Pd/Al_2O_3 catalyst, and Pd/MgO catalyst

of highly dispersed PdO species. There were no hydrogen consumption peaks in the TPR profile of $MgAl_2O_4$, suggesting that the $MgAl_2O_4$ supports were not reducible. For the Pd/$MgAl_2O_4$ catalyst, the first reduction peak at 34 ℃ was obviously larger than that of Pd/MgO catalyst and Pd/Al_2O_3 catalyst, which was agreed with its higher metal dispersion results in HAADF-STEM and CO-chemisorption results [32]. Furthermore, the reduction peak over Pd/$MgAl_2O_4$ catalyst would tend to shift to a higher temperature because of a stronger interaction between Pd species and $MgAl_2O_4$ support [31, 33]. On the one hand, the stronger interactions would enhance the metal dispersion for metal-support interfaces increasement and tune the electronic properties of Pd species, enhancing their catalytic performance. On the other hand, the stronger interactions between Pd and $MgAl_2O_4$ would hinder the reduction of PdO_x [33–35] that is regarded as the major active phase under oxidation condition [36]. Therefore, the $MgAl_2O_4$ support is responsible for dispersing the Pd species and maintaining its suitable chemical state via Pd-$MgAl_2O_4$ interface.

3.3.2 MeOH-TPSR Characterization

The MeOH-TPSR experiments were carried out to investigate the methanol activation ability without atomosphere oxygen, assisted with the oxygen vacancies in the support. Figure 5 shows the profiles of MeOH-TPSR without oxygen over four samples. The temperature where methanol begins to activate and be completely transformed was investigated to reflect its activation ability. As shown in Fig. 5, $MgAl_2O_4$ support would tend to activate the methanol at 390 ℃ and completely convert methanol into CO_2 at 575 ℃ with the assistance of oxygen vancancies in the spinel oxide [18, 29, 30]. However, the beginning activation temperature of the Pd/$MgAl_2O_4$ catalyst was reduced to 80 ℃ with a completely transformed temperature at 320 ℃ with a synergistic between Pd species and $MgAl_2O_4$. Compared with Pd/MgO catalyst and Pd/Al_2O_3 catalyst, the Pd/$MgAl_2O_4$ catalyst has a stronger methanol activation ability. Furthermore, the beginning activation temperature on these samples was correlated very well with their activity order, implying that the methanol oxidation reaction over Pd catalysts followed the Mars van Krevelen (MvK) mechanism and the surface oxygen on the catalysts participated in the methanol oxidation process [33].

3.3.3 CO-DRIFTS Characterization

The electronic properties of Pd species are easily changed when characterized via traditional *ex-situ* methods, which provides misleading information for the reaction mechanism investigation. In this study, the CO-DRIFTS was performed to investigate the chemical properties of the catalysts using CO as a probe molecule under *in-situ* conditions [37]. As shown in Fig. 6a, the adsorption peaks at 1800–1950 cm^{-1} and 2000–2150 cm^{-1} corresponded to the bridge bonded CO to Pd^0 (B peak) and the linear bonded CO to Pd^0 (L peak) [38, 39], respectively. The bridge bonded CO (B peak) was assigned to the larger Pd particle size, while the linear bonded CO (L peak) was assigned to high dispersed Pd sites [31, 40, 41]. Figure 6b compared the ratio of the two bonds over three catalysts by calculating the peak areas (linear bonded/bridge bonded, named L/B). The ratio of linear bond area to bridge bond area decreased from 38.4% to 8.1% and 1.3% over Pd/$MgAl_2O_4$ catalyst, Pd/Al_2O_3 catalyst and Pd/Al_2O_3 catalyst. These results would verify the smaller Pd particle size and higher Pd dispersion over $MgAl_2O_4$. And the order is agreed with the catalytic performance, which illustrates that Pd dispersion would have a great impact on the oxidation reaction. On one hand, the higher Pd dispersion provides a more abundant Pd-support interface for

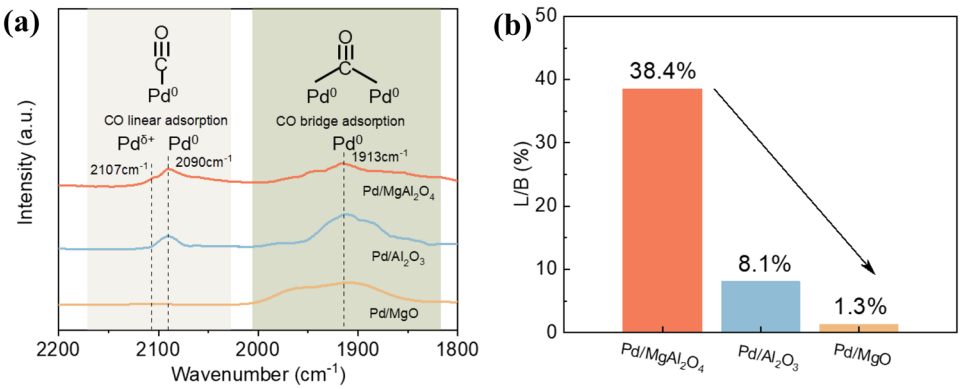

Fig. 6 **a** CO-DRIFTS and **b** the ratio of L/B peak over Pd/$MgAl_2O_4$ catalyst, Pd/Al_2O_3 catalyst, and Pd/MgO catalyst

molecule adsorb and transformation [42]. On other hand, the electronic state of Pd species could be easily tunned with higher dispersion due to the strong metal-support interaction [33, 43].

Furthermore, there was a shoulder peak at ~ 2100 cm^{-1}, which is assigned to linearly adsorbed CO on $Pd^{\delta+}$ that is in direct contact with oxygen [44, 45] over spinel oxide. It is suggested that the high density of oxygen vacancies (O_v) over $MgAl_2O_4$ could effectively stabilize the Pd species via $Pd^{\delta+}$—O_v bond, which has been reported in other catalyst systems [46]. The stronger interaction between Pd and $MgAl_2O_4$ would hinder the reduction of PdO_x, enhancing its catalytic performance during the reaction. Therefore, the stronger interaction, confirmed by CO-DRIFTS, would maintain the optimized Pd electronic state over $MgAl_2O_4$, forming Pd-$MgAl_2O_4$ interface.

3.3.4 *In-situ* DRIFTS Characterization

In-situ DRIFTS spectra were carried out to study the mechanism via characterizing the surface species and intermediates. In this work, different gases (CH_3OH and $CH_3OH + O_2$) were switched into the reactor and observed the behaviors of the surface species, as shown in Fig. 7. The intense bands at ~ 1928 cm^{-1} and ~ 1832 cm^{-1} were associated with methoxy. The features presented at ~ 1370 cm^{-1} associated with

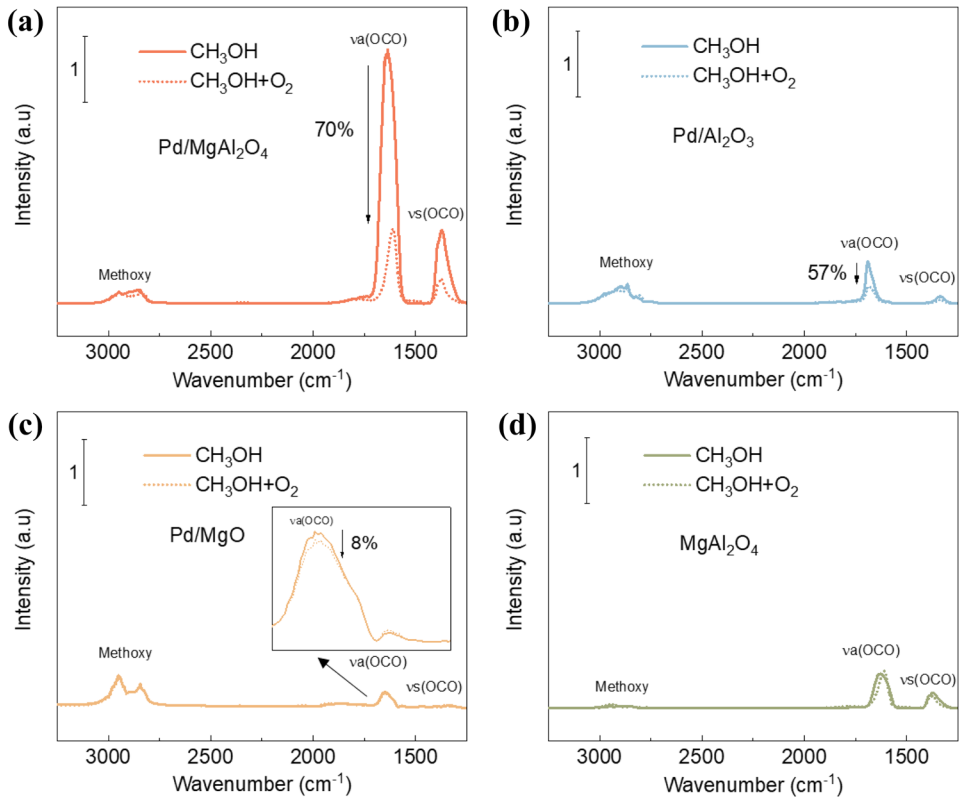

Fig. 7 *In-situ* DRIFTS spectra over **a** Pd/$MgAl_2O_4$ catalyst; **b** Pd/Al_2O_3 catalyst; **c** Pd/MgO catalyst, and **d** $MgAl_2O_4$ with CH_3OH and CH_3OH/O_2

v_s(OCO), and ~ 1564 cm^{-1} associated with v_a(OCO), both representing bidentate formate bound [28, 47]. When the catalysts were exposed to CH_3OH gas, the bidentate formate appeared. It is indicated that the methanol could react with the oxygen vacancies. For the Pd/$MgAl_2O_4$ catalyst, the signal intensity of bidentate formate was greatly significant larger than that of Pd/MgO catalyst and Pd/Al_2O_3 catalyst, which resulted from the higher density of oxygen vacancies in the spinel oxide. The oxygen vacancy would enhance the absorption of methanol and its conversion to bidentate formate [48, 49]. It was also confirmed via MeOH-TPSR experiments without oxygen assistance.

When O_2 is fed into the reactor, the bidentate formate species was quickly decreased over catalysts as shown in Fig. 7a-c. The intensity was decreased 70% over the Pd/$MgAl_2O_4$ catalyst, then followed Pd/Al_2O_3 catalyst (57%) and Pd/MgO catalyst (8%), which is agreed with their catalytic performance. The bidentate formate reaction may be the key process for the methanol oxidation reactions [49]. However, the bidentate formate over pure $MgAl_2O_4$ support was almost not transformed at 200 ℃. Thus, the Pd species over the support would play a capital role for the intermediate transformation. There is a synergistic effect between the Pd species and $MgAl_2O_4$ support: the abundant oxygen vacancies in the $MgAl_2O_4$ enhance the methanol absorption, forming bidentate formate; the highly dispersed Pd species would convert the intermediate into final CO_2 with the assistance of oxygen. So, the abundant Pd-$MgAl_2O_4$ interface provides different active site for the methanol oxidation.

4 Conclusion

In this work, a novel Pd/$MgAl_2O_4$ catalyst was prepared and compared its catalytic performance for the methanol oxidation over Pd/Al_2O_3 catalyst and Pd/MgO catalyst. The Pd/$MgAl_2O_4$ catalyst could achieve 100% methanol oxidation at 198 ℃, which shows a huge industrial application potential. A series of textural characterizations, including HRTEM, XRD, CO-chemisorption, and H_2-TPR show that Pd was uniformly distributed over the $MgAl_2O_4$ support, forming Pd-$MgAl_2O_4$ interface due to a strong interaction. The MeOH-TPSR, CO-DRIFTS and i*n-situ* DRIFTS show that a synergistic effect between the Pd species and $MgAl_2O_4$ support enhanced its catalytic performance: the methanol tended to be absorbed on $MgAl_2O_4$ support with abundant oxygen vacancies, forming bidentate formate; the highly dispersed Pd species would convert the bidentate formate with the assistance of oxygen. This study prepared a novel methanol oxidation catalyst via constructing Pd-$MgAl_2O_4$ interface and its comprehensive mechanism studies provide an opportunity to design superior catalysts for VOCs removal.

Supplementary Information The online version contains supplementary material available at https://doi.org/10.1007/s10562-022-04107-y.

Acknowledgements This work was supported by the National Natural Science Foundation of China [Grant Number 42107054].

Funding National Natural Science Foundation of China,42107054

Declarations

Conflict of interest The authors declare that they have no known competing financial interests or personal relationships that could have appeared to influence the work reported in this paper.

References

1. Billionnet C, Gay E, Kirchner S, Leynaert B, Annesi-Maesano I (2011) Quantitative assessments of indoor air pollution and respiratory health in a population-based sample of French dwellings. Environ Res 111(3):425–434. https://doi.org/10.1016/j.envres.2011.02.008
2. Hosseini M, Barakat T, Cousin R, Aboukaïs A, Su BL, De Weireld G, Siffert S (2012) Catalytic performance of core–shell and alloy Pd–Au nanoparticles for total oxidation of VOC: the effect of metal deposition. Appl Catal B 111–112:218–224. https://doi.org/10.1016/j.apcatb.2011.10.002
3. Calzada LA, Collins SE, Han CW, Ortalan V, Zanella R (2017) Synergetic effect of bimetal-lic Au-Ru/TiO_2 catalysts for complete oxidation of methanol. Appl Catal B 207:79–92. https://doi.org/10.1016/j.apcatb.2017.01.081
4. Luo Y, Xiao Y, Cai G, Zheng Y, Wei K (2012) Performance of $Ce_{0.25}Zr_{0.75}O_2$ promoted Pd/Ag/γ-Al_2O_3 catalysts for low-temperature methanol oxidation. Fuel 93:533–538. https://doi.org/10.1016/j.fuel.2011.10.027
5. Kim M-Y, Kyriakidou EA, Choi J-S, Toops TJ, Binder AJ, Thomas C, Parks JE, Schwartz V, Chen J, Hensley DK (2016) Enhancing low-temperature activity and durability of Pd-base diesel oxidation catalysts using ZrO_2 supports. Appl Catal B 187:181–194. https://doi.org/10.1016/j.apcatb.2016.01.023
6. Kim C, Hong E, Shin C-H (2019) Improvement of methane combustion activity for Pd/ZrO_2 catalyst by simple reduction/reoxidation treatment. Catalysts 9(10):838. https://doi.org/10.3390/catal9100838
7. Dasireddy VDBC, Likozar B (2019) The role of copper oxidation state in Cu/ZnO/Al_2O_3 catalysts in CO_2 hydrogenation and methanol productivity. Renew Energ 140:452–460. https://doi.org/10.1016/j.renene.2019.03.073
8. Li Q, Li F-t (2020) Recent advances in surface and interface design of photocatalysts for the degradation of volatile organic compounds. Adv Colloid Interface Sci 284:102275. https://doi.org/10.1016/j.cis.2020.102275
9. Huang G, Liu L, Chen L, Gao L, Zhu J, Fu H (2022) Unique insights into photocatalytic VOCs oxidation over WO_3/carbon dots nanohybrids assisted by water activation and electron transfer at interfaces. J Hazard Mater 423:127134. https://doi.org/10.1016/j.jhazmat.2021.127134
10. Mahmood A, Shi G, Wang Z, Rao Z, Xiao W, Xie X, Sun J (2021) Carbon quantum dots-TiO_2 nanocomposite as an efficient photocatalyst for the photodegradation of aromatic ring-containing mixed VOCs: An experimental and DFT studies of adsorption and electronic structure of the interface. J Hazard Mater 401:123402. https://doi.org/10.1016/j.jhazmat.2020.123402

11. Wang Q, Li Y, Serrano-Lotina A, Han W, Portela R, Wang R, Banares MA, Yeung KL (2021) Operando investigation of toluene oxidation over 1D Pt@CeO_2 derived from Pt cluster-containing MOF. J Am Chem Soc 143(1):196–205. https://doi.org/10.1021/jacs.0c08640
12. Wang Q, Li Z, Banares MA, Weng LT, Gu Q, Price J, Han W, Yeung KL (2019) A novel approach to high-performance alio-valent-substituted catalysts-2D bimetallic MOF-derived $CeCuO_x$ microsheets. Small 15(42):e1903525. https://doi.org/10.1002/smll.201903525
13. Jabłońska M, Król A, Kukulska-Zając E, Tarach K, Girman V, Chmielarz L, Góra-Marek K (2015) Zeolites Y modified with palladium as effective catalysts for low-temperature methanol incineration. Appl Catal B 166–167:353–365. https://doi.org/10.1016/j.apcatb.2014.11.047
14. Zhang Z, Chen M, Jiang Z, Shangguan W (2011) Low-temperature selective catalytic reduction of NO with propylene in excess oxygen over the Pt/ZSM-5 catalyst. J Hazard Mater 193:330–334. https://doi.org/10.1016/j.jhazmat.2011.07.038
15. Kucherov AV, Sinev IM, Ojala S, Keiski R, Kustov LM (2007) Adsorptive-catalytic removal of CH_3OH, CH_3SH, and CH_3SSCH_3 from air over the bifunctional system noble metals/HZSM-5. Stud Surf Sci Catal 170:1129–1136. https://doi.org/10.1016/S0167-2991(07)80969-4
16. Fan L, Wang K, Xu K, Liang Z, Wang H, Zhou SF, Zhan G (2020) Structural isomerism of two Ce-BTC for fabricating Pt/CeO_2 nanorods toward low-temperature CO oxidation. Small 16(40):e2003597. https://doi.org/10.1002/smll.202003597
17. Zhao Q, Yan Z, Chen C, Chen J (2017) Spinels: controlled preparation, oxygen reduction/evolution reaction application, and beyond. Chem Rev 117(15):10121–10211. https://doi.org/10.1021/acs.chemrev.7b00051
18. Liu T, Xu D, Wu D, Liu G, Hong X (2021) Spinel $ZnFe_2O_4$ regulates copper sites for CO_2 hydrogenation to methanol. ACS Sustain Chem Eng 9(11):4033–4041. https://doi.org/10.1021/acssuschemeng.0c07682
19. Dasireddy VDBC, Neja SŠ, Blaž L (2018) Correlation between synthesis pH, structure and Cu/MgO/Al_2O_3 heterogeneous catalyst activity and selectivity in CO_2 hydrogenation to methanol. J CO2 Util 28:189–199. https://doi.org/10.1016/j.jcou.2018.09.002
20. Dasireddy VDBC, Likozar B (2022) Cu–Mn–O nano-particle/nano-sheet spinel-type materials as catalysts in methanol steam reforming (MSR) and preferential oxidation (PROX) reaction for purified hydrogen production. Renew Energ 182:713–724. https://doi.org/10.1016/j.renene.2021.10.033
21. Kaczmarczyk J, Zasada F, Janas J, Indyka P, Piskorz W, Kotarba A, Sojka Z (2016) Thermodynamic stability, redox properties, and reactivity of Mn_3O_4, Fe_3O_4, and Co_3O_4 model catalysts for N_2O decomposition: Resolving the origins of steady turnover. ACS Catal 6(2):1235–1246. https://doi.org/10.1021/acscatal.5b02642
22. PalDey S, Gedevanishvili S, Zhang W, Rasouli F (2005) Evaluation of a spinel based pigment system as a CO oxidation catalyst. Appl Catal B 56(3):241–250. https://doi.org/10.1016/j.apcatb.2004.09.013
23. Evdou A, Zaspalis V, Nalbandian L (2016) Ferrites as redox catalysts for chemical looping processes. Fuel 165:367–378. https://doi.org/10.1016/j.fuel.2015.10.049
24. Martin A, Luck F, Armbruster U, Patria L, Radnik J, Schneider M (2005) Ammonia removal from effluent streams of wet oxidation under high pressure. Top Catal 33(1–4):155–169. https://doi.org/10.1007/s11244-005-2522-4
25. Araiza DG, Gómez-Cortés A, Díaz G (2017) Reactivity of methanol over copper supported on well-shaped CeO_2: A TPD-DRIFTS study. Catal Sci Technol 7(22):5224–5235. https://doi.org/10.1039/C7CY00984D
26. Cao T, You R, Zhang X, Chen S, Li D, Zhang Z, Huang W (2018) An in situ DRIFTS mechanistic study of CeO_2-catalyzed acetylene semihydrogenation reaction. Phys Chem Chem Phys 20(14):9659–9670. https://doi.org/10.1039/C8CP00668G
27. Huttunen PK, Labadini D, Hafiz SS, Gokalp S, Wolff EP, Martell SM, Foster M (2021) DRIFTS investigation of methanol oxidation on CeO_2 nanoparticles. Appl Surf Sci. https://doi.org/10.1016/j.apsusc.2021.149518
28. Kattel S, Yan B, Yang Y, Chen JG, Liu P (2016) Optimizing binding energies of key intermediates for CO_2 hydrogenation to methanol over oxide-supported copper. J Am Chem Soc 138(38):12440–12450. https://doi.org/10.1021/jacs.6b05791
29. Bahmanpour AM, Héroguel F, Kılıç M, Baranowski CJ, Schouwink P, Röthlisberger U, Luterbacher JS, Kröcher O (2020) Essential role of oxygen vacancies of Cu-Al and Co-Al spinel oxides in their catalytic activity for the reverse water gas shift reaction. Appl Catal B 266:118669. https://doi.org/10.1016/j.apcatb.2020.118669
30. Castellanos-Beltran IJ, Perreault L-S, Braidy N (2021) Application of Ni–spinel in the chemical-looping conversion of CO_2 to CO via induction-generated oxygen vacancies. J Phys Chem C 125(13):7213–7226. https://doi.org/10.1021/acs.jpcc.1c00928
31. Wang W, Zhang H-b, Lin G-d, Xiong Z-t (2000) Study of Ag/$La_{0.6}Sr_{0.4}MnO_3$ catalysts for complete oxidation of methanol and ethanol at low concentrations. Appl Catal B 24(3):219–232. https://doi.org/10.1016/S0926-3373(99)00106-X
32. Lippits MJ, Boer Iwema RRH, Nieuwenhuys BE (2009) A comparative study of oxidation of methanol on γ-Al_2O_3 supported group IB metal catalysts. Catal Today 145(1):27–33. https://doi.org/10.1016/j.cattod.2008.07.018
33. Yang Z, Liang S, Sun L, Hu X, Fang W, Lai W, Yi X (2021) Highly active and stable Pd/$MgAl_2O_4$@MgO catalyst with electronic metal-support interaction for selective hydrogenation of isoprene. Fuel. https://doi.org/10.1016/j.fuel.2020.119920
34. Jiang F, Wang S, Liu B, Liu J, Wang L, Xiao Y, Xu Y, Liu X (2020) In-sights into the influence of CeO_2 crystal facet on CO_2 hydrogenation to methanol over Pd/CeO_2 catalysts. ACS Catal 10(19):11493–11509. https://doi.org/10.1021/acscatal.0c03324
35. Yang J, Peng M, Ren G, Qi H, Zhou X, Xu J, Deng F, Chen Z, Zhang J, Liu K, Pan X, Liu W, Su Y, Li W, Qiao B, Ma D, Zhang T (2020) A hydrothermally stable irreducible oxide-modified Pd/$MgAl_2O_4$ catalyst for methane combustion. Angew Chem Int Ed Engl 59(42):18522–18526. https://doi.org/10.1002/anie.202009050
36. Bruix A, Migani A, Vayssilov GN, Neyman KM, Libuda J, Illas F (2011) Effects of deposited Pt particles on the reducibility of CeO_2(111). Phys Chem Chem Phys 13(23):11384–11392. https://doi.org/10.1039/C1CP20950G
37. Vayssilov GN, Lykhach Y, Migani A, Staudt T, Petrova GP, Tsud N, Skála T, Bruix A, Illas F, Prince KC, Matolı´n Vr, Neyman KM, Libuda J, (2011) Support nanostructure boosts oxygen transfer to catalytically active platinum nanoparticles. Nat Mater 10(4):310–315. https://doi.org/10.1038/nmat2976
38. Chin Y-H, Buda C, Neurock M, Iglesia E (2013) Consequences of metal–oxide interconversion for C-H bond activation during CH_4 reactions on Pd catalysts. J Am Chem Soc 135(41):15425–15442. https://doi.org/10.1021/ja405004m
39. Wang Q, Tichit D, Meunier F, Guesmi H (2020) Combined DRIFTS and DFT study of CO adsorption and segregation modes in Pt–Sn nanoalloys. J Phys Chem C 124(18):9979–9989. https://doi.org/10.1021/acs.jpcc.0c01296
40. Ding D, Xu X, Tian P, Liu X, Xu J, Han Y-F (2018) Promotional effects of Sb on Pd-based catalysts for the direct synthesis of hydrogen peroxide at ambient pressure. Chinese J Catal 39(4):673–681. https://doi.org/10.1016/S1872-2067(18)63031-1

41. Cao Y, Sui Z, Zhu Y, Zhou X, Chen D (2017) Selective hydrogenation of acetylene over Pd-In/Al_2O_3 catalyst: promotional effect of indium and composition-dependent performance. ACS Catal 7(11):7835–7846. https://doi.org/10.1021/acscatal.7b01745
42. Liu J, Wang L, Okejiri F, Luo J, Zhao J, Zhang P, Liu M, Yang S, Zhang Z, Song W, Zhu W, Liu J, Zhao Z, Feng G, Xu C, Dai S (2020) Deep understanding of strong metal interface confinement: a journey of Pd/FeO_x catalysts. ACS Catal 10(15):8950–8959. https://doi.org/10.1021/acscatal.0c01447
43. Chen H, Shuang H, Lin W, Li X, Zhang Z, Li J, Fu J (2021) Tuning interfacial electronic properties of palladium oxide on vacancy-abundant carbon nitride for low-temperature dehydrogenation. ACS Catal 11(10):6193–6199. https://doi.org/10.1021/acscatal.1c00712
44. Sun K, Lu W, Wang M, Xu X (2004) Characterization and catalytic performances of La doped Pd/CeO_2 catalysts for methanol decomposition. Appl Catal A 268(1):107–113. https://doi.org/10.1016/j.apcata.2004.03.020
45. Zhou G-F, Ma J, Bai S, Wang L, Guo Y (2020) CO catalytic oxidation over Pd/CeO_2 with different chemical states of Pd. Rare Met 39(7):800–805. https://doi.org/10.1007/s12598-019-01347-7
46. Chen AL, Yu XJ, Zhou Y, Miao S, Li Y, Kuld S, Sehested J, Liu JY, Aoki T, Hong S, Camellone MF, Fabris S, Ning J, Jin CC, Yang CW, Nefedov A, Woll C, Wang YM, Shen WJ (2019) Structure of the catalytically active copper-ceria interfacial perimeter. Nat Catal 2(4):334–341. https://doi.org/10.1038/s41929-019-0226-6
47. Cao S, Yang M, Elnabawy AO, Trimpalis A, Li S, Wang C, Goltl F, Chen Z, Liu J, Shan J, Li M, Haas T, Chapman KW, Lee S, Allard LF, Mavrikakis M, Flytzani-Stephanopoulos M (2019) Single-atom gold oxo-clusters prepared in alkaline solutions catalyse the heterogeneous methanol self-coupling reactions. Nat Chem 11(12):1098–1105. https://doi.org/10.1038/s41557-019-0345-3
48. Dostagir NHMD, Rattanawan R, Gao M, Ota J, Hasegawa J-y, Asakura K, Fukouka A, Shrotri A (2021) Co single atoms in ZrO_2 with inherent oxygen vacancies for selective hydrogenation of CO_2 to CO. ACS Catal 11(15):9450–9461. https://doi.org/10.1021/acscatal.1c02041
49. Yue Y, Li Y, Wang T, Wang S, Han L, Du C (2022) Enhancement of methanol oxidation performance over Pd/CeO_2 derived from MOF and mechanism investigation via in situ studies. Catal Lett. https://doi.org/10.1007/s10562-021-03901-4

Authors and Affiliations

Wei Zhao[1] · Hongyi Zhang[2] · Lei Zhang[3] · Jianchao Gong[1] · Tianen Chen[1] · Liming Ren[4] · Yaxiong Ji[1,5] · Fanbin Meng[4]

✉ Yaxiong Ji
jiyx20@mails.tsinghua.edu.cn

✉ Fanbin Meng
mfb1469@163.com

[1] Hoffmann Institute of Advanced Materials, Shenzhen Polytechnic, Shenzhen 518055, People's Republic of China

[2] Western Christian High School, Upland, CA 91786, USA

[3] Ulink College of Shanghai, Shanghai 201615, People's Republic of China

[4] Research Institute of Petroleum Processing, SINOPEC Group, Beijing 100084, People's Republic of China

[5] Tsinghua Shenzhen International Graduate School, Tsinghua University, Shenzhen 518055, People's Republic of China